Detection of Functional Communities in Networks of Randomly Coupled Oscillators Using the Dynamic-Mode Decomposition

Christopher W. Curtis
*Department of Mathematics and Statistics, San Diego State University**

Mason A. Porter
Department of Mathematics, University of California, Los Angeles

Dynamic-mode decomposition (DMD) is a versatile framework for model-free analysis of time series that are generated by dynamical systems. We develop a DMD-based algorithm to investigate the formation of "functional communities" in networks of coupled, heterogeneous Kuramoto oscillators. In these functional communities, the oscillators in the network have similar dynamics. We consider two common random-graph models (Watts–Strogatz networks and Barabási–Albert networks) with different amounts of heterogeneities among the oscillators. In our computations, we find that membership in a community reflects the extent to which there is establishment and sustainment of locking between oscillators. We construct forest graphs that illustrate the complex ways in which the heterogeneous oscillators associate and disassociate with each other.

I. INTRODUCTION

Researchers in myriad disciplines employ networks to represent entities (i.e., nodes) that interact with each other through their connections (which are encoded by edges) [1]. Network architecture, in turn, affects the dynamics of systems that evolve on networks [2]. Network structure can profoundly impact the spread of diseases [3] and information [4], the collective behavior of coupled oscillators [5, 6], and more.

The analysis of networks plays an increasingly important role throughout the sciences and engineering, and this is very prominent in the study of dynamical systems [1, 7]. A key question is how interacting entities in a network form collectives known as *communities*, which can take the form of either *structural* or *functional* communities. A *structural community* is a dense set of nodes that is connected sparsely to other dense sets of nodes [8, 9]. A very large number of approaches have been developed to algorithmically detect structural communities in networks. By contrast, considerably less effort has been devoted to the detection of *functional communities*. One way to detect functional communities is by running a dynamical process on a network, constructing a new network (a so-called "functional network") based on time-series similarity of the outputs of the network's nodes, and then detecting structural communities in the functional network [10, 11]. One can also detect functional communities using time-series output of experiments. Whether the time-series output comes from a model or experimental measurements, the focus in functional-community detection is behavioral similarity of a network's entities over time.

In this paper, we are concerned with the setting of coupled oscillators on networks. The network itself may have community structure (which is based on its structural communities), and one can examine it through one or more of the myriad available methods for community detection [9]. Additionally, by examining the output of such a dynamical system and tracking phenomena such as synchronization, one can also study the same system's functional community structure. This topic was explored by Arenas et al. [10] through an investigation of coupled Kuramoto oscillators on networks. The fact that coupled Kuramoto models have been studied so extensively [6] makes then an ideal test case for studies of functional-community detection in coupled oscillators, with a view towards extending such analysis to other systems (including experimental ones, such as when studying neuroimaging data [11]). In our work, we have coupled oscillators in mind, but other types of dynamical systems on networks can also have functional communities [12].

Arenas et al. [10] examined Kuramoto oscillators that are coupled to each other on a network with a hierarchical community structure (with small, denser communities nested inside larger, sparser ones), and they examined how the architecture of structural communities affects the formation of functional communities, as quantified by how long it takes oscillators to synchronize. Oscillators in denser communities synchronize faster than oscillators in sparser ones. Variations of coupled Kuramoto oscillators have also been used to study of functional communities [13, 14]. In these papers, the network architecture was fixed, and the key question concerned constructing partitions of networks that are based on oscillator dynamics.

Our investigation of functional communities in the present paper departs from the perspective of the aforementioned papers, as we focus directly on detecting communities from output dynamics. We consider both the formation and the disappearance of functional communities. Instead of examining synchronization time scales as a way to partition a network of oscillators, we generate output data from coupled Kuramoto oscillators on networks (which we construct from random-graph mod-

* ccurtis@sdsu.edu

els) and identify functional communities from such data. These functional communities, whose name takes inspiration from studies of functional brain networks in neuroscience [11], arise from communities in networks in which edges encode time-series similarity of the nodes of some network. Another name for such communities is "behavioral communities", and they were explored briefly in [15] using methods from information theory and structural community detection.

To detect functional communities in a model-free way, we use the modal-decomposition technique known as dynamic-mode decomposition (DMD). For more information about DMD, see [16–18] for comprehensive reviews and [19–21] for further surveys and discussions of recent extensions. The primary benefit of the DMD is that it is a model-free data-processing tool that allows one to generate modal decompositions from arbitrarily complicated data sets. Moreover, in contrast to other data-analysis methods (such as principle-component analysis), DMD also gives a convenient mechanism for generating models from measured data alone, and it thereby gives a way to sidestep model development in situations in which it is difficult or even impossible. However, DMD requires the introduction of an infinite-dimensional framework, as one needs to study the spectral properties of an associated Koopman operator [22].

Our DMD-based approach provides a straightforward and flexible way to generate functional communities from a time series. The formation of such communities still relies on synchronization of certain subsets of the oscillators of a network, but we accomplish this goal without observing any global attractors (at least on the time scales that we examine). Our approach thereby gives a flexible and adaptive method for identifying functional communities in large sets of time series of coupled nonlinear oscillators, and we anticipate that it will also be applicable to wider classes of time series in which community formation is of interest. Our work complements the recent results of Kunert-Graf et al. [23], who used unsupervised learning techniques to cluster DMD modes to capture spatially and temporarily coherent patterns in complex signals. Our code is available at https://github.com/cwcurtis/DMD_Community_Detect.

Our paper proceeds as follows. In Section II, we give the necessary background and definitions to understand both DMD and how we generate our data. In Section III, we explain our algorithm for the detection of functional communities. In Section IV, we present the results of our numerical experiments. Finally, in Section V, we summarize our results and and discuss future work.

II. BACKGROUND AND DEFINITIONS

A. Dynamic-Mode Decomposition

Consider a nonlinear dynamical system of the form

$$\frac{d\mathbf{y}}{dt} = f(\mathbf{y}, t)\,, \quad \mathbf{y}(0) = \mathbf{x} \in \mathbb{R}^{N_s}\,. \tag{1}$$

We denote the affiliated flow of (1) by $\mathbf{y}(t) = \varphi(t;\mathbf{x})$. The associated Hilbert space of observables is $L_2\left(\mathbb{R}^{N_s}, \mathbb{R}, \mu\right)$, for which we use the shorthand notation $L_2(\mathcal{O})$, where a function $g : \mathbb{R}^{N_s} \longrightarrow \mathbb{R}$ satisfies $g \in L_2(\mathcal{O})$ if

$$\int_{\mathbb{R}^{N_s}} |g(\mathbf{x})|^2 \, d\mu(\mathbf{x}) < \infty$$

for some appropriate measure μ.

One can gain considerable insight by examining the associated linear representation of the problem. This representation is given by the infinite-dimensional Koopman operator

$$\mathcal{K}^t : L_2(\mathcal{O}) \to L_2(\mathcal{O})\,.$$

For $g \in L_2(\mathcal{O})$, we have that

$$\mathcal{K}^t g(\mathbf{x}) = g\left(\varphi(t;\mathbf{x})\right)\,.$$

The power of moving to a linear-operator framework is that we capture the dynamics of the nonlinear system 1, as measured via observables, using the eigenvalues of $\mathcal{K}^t$. We assume that $\mathcal{K}^t$ has a discrete spectrum. If we can find a basis of $g \in L_2(\mathcal{O})$ via the Koopman eigenfunctions h_j, which satisfy

$$\mathcal{K}^t h_j = e^{t\lambda_j} h_j\,,$$

then it follows for any other observable g that

$$g = \sum_{j=1}^{\infty} c_j h_j\,, \quad \mathcal{K}^t g = \sum_{j=1}^{\infty} e^{t\lambda_j} c_j h_j\,. \tag{2}$$

It is typically impossible to determine the modes of the Koopman operator $\mathcal{K}^t$ in closed form. Therefore, scholars have developed the dynamic-mode decomposition (DMD) [16–18] and extended dynamic-mode decomposition (EDMD)[24, 25] to yield methods for the practical numerical computation of a finite number of the Koopman modes.

To do DMD, we start by sampling the flow $\varphi(t;\mathbf{x})$ at a discrete times $t_j = t_i + (j-1)\delta t$, where $j = 1, \ldots, N_T + 1$ to generate a data set $\mathbf{y}_j = \varphi(t_j, \mathbf{x})$. If we select the set $\mathbf{g} = \{g_l\}_{l=1}^{M}$ of observables such that $g_l(\mathbf{x}_l) = x_l$, then the DMD approximates $\mathcal{K}^{\delta t}$ by computing the spectra of the finite-dimensional operator $\tilde{K}_a$ that we obtain by solving the optimization problem

$$\mathbf{K}_a = \arg\min_{\mathbf{K}} \|\mathbf{Y}_+ - \mathbf{K}\mathbf{Y}_-\|_F^2\,,$$

where

$$\mathbf{Y}_- = [\mathbf{y}_1\ \mathbf{y}_2 \cdots \mathbf{y}_{N_T}]\ , \quad \mathbf{Y}_+ = [\mathbf{y}_2\ \mathbf{y}_3 \cdots \mathbf{y}_{N_T+1}]\ .$$

After obtaining the $N_s \times N_s$ matrix $\mathbf{K}_a$, we compute its singular-value decomposition (SVD) $\mathbf{K}_a = \mathbf{U}\mathbf{\Sigma}\mathbf{V}^\dagger$ [26], where each factor is an $N_s \times N_s$ matrix, $\mathbf{U}$ and $\mathbf{V}$ are unitary, $\mathbf{\Sigma}$ is diagonal, and † denotes the Hermitian conjugate. Following the standard convention, we order the diagonal entries $\sigma_1, \ldots, \sigma_M$ (i.e., the singular values) of $\mathbf{\Sigma}$ so that

$$\sigma_1 \geq \sigma_2 \geq \cdots \geq \sigma_M \geq 0\,.$$

We then define the diagonal matrix $\tilde{\mathbf{\Sigma}}$ with diagonal entries

$$\tilde{\sigma}_j = \begin{cases} \sigma_j, & \log_{10}\left(\frac{\sigma_j}{\sigma_1}\right) \geq t_{\mathrm{DMD}} \\ 0, & \log_{10}\left(\frac{\sigma_j}{\sigma_1}\right) < t_{\mathrm{DMD}}\,, \end{cases} \tag{3}$$

where we set the DMD threshold t_{DMD} to remove singular values that are more reflective of ill-conditioning in $\mathbf{K}_a$ than of meaningful information. To be useful in practice, we take $t_{\mathrm{DMD}} < 0$. We then work with the matrix $\tilde{\mathbf{K}}_a = \mathbf{U}\tilde{\mathbf{\Sigma}}\mathbf{V}^\dagger$. See [27] for a discussion of this DMD method and related approaches.

We let $\tilde{\mathbf{K}}_a = \mathbf{\Xi} e^{\delta t \mathbf{\Lambda}} \mathbf{\Xi}^{-1}$ and write

$$\mathbf{y}_j = \sum_{n=1}^{M} \xi_n e^{j\delta t \lambda_n} h_n(\mathbf{x})\,, \quad h_n(\mathbf{x}) = \left(\mathbf{\Xi}^{-1}\mathbf{x}\right)_n\ .$$

The real part of the eigenvalue λ_n gives the amplitude of the nth mode, and the imaginary part of λ_n gives its oscillation frequency. We find the evolution of the associated eigenfunctions of the Koopman operator using the formula

$$h_n(\mathbf{y}_j) = \left(\mathbf{\Xi}^{-1}\mathbf{y}_j\right)_n\ .$$

A measure of error is the extent to which the computed modes $h_n(\mathbf{x})$ behave as Koopman eigenfunctions [21]. To quantify this, we follow [28] and calculate

$$\mathcal{E}_j = \frac{\sum_{n=1}^{N_T} \left| h_j\left(\mathbf{y}_{n+1}\right) - e^{\delta t \lambda_j} h_j\left(\mathbf{y}_n\right)\right|}{\sum_{n=1}^{N_T} \left| h_j\left(\mathbf{y}_n\right)\right|}$$

for each $j \in \{1, \ldots, N_T + 1\}$. The quantity $\mathcal{E}_j$ gives a normalized measure of how well the computed approximations to the Koopman eigenfunctions and eigenvalues are able to linearize the dynamics as the exact ones in (2). We choose a tolerance ϵ_m and keep only the modes that satisfy $\mathcal{E}_j < \epsilon_m$. We denote the number of the modes that we keep by N_r. We enforce how well these N_r modes reconstruct the time series by choosing a reconstruction-error parameter ϵ_{rc} so that

$$\frac{\|\mathbf{Y}_+ - \mathbf{H}\|_F}{\|\mathbf{Y}_+\|_F} < \epsilon_{rc}\,,$$

where H is the matrix with columns

$$\mathbf{h}_j = \sum_{l=1}^{N_r} \xi_{n_l} e^{j\delta t \lambda_{n_l}} h_{n_l}(\mathbf{x})$$

and n_l denotes the subset of modes that satisfy the criterion $\mathcal{E}_{n_l} < \epsilon_m$.

There is an interplay between the choices of t_{DMD}, ϵ_m, and ϵ_{rc}. It takes effort (e.g., through trial and error) to balance these parameters to produce meaningful results. For example, if t_{DMD} is too small (e.g., $t_{\mathrm{DMD}} = -16$, which corresponds to machine precision on most desktop computers), then one typically corrupts a DMD computation to the point that there is no practical way to find reasonable choices of ϵ_m or ϵ_{rc}. However, if t_{DMD} is too large, only a very small number of modes meet the ϵ_m criterion, rendering it difficult to make reasonable choices of ϵ_{rc}. Likewise, setting ϵ_m to a value that is too small can produce excellent approximations to Koopman modes, but it is hard for the modal reconstruction to allow reasonable choices of ϵ_{rc}. In Section IV, we describe parameter choices that reflect the necessary balancing.

B. Coupled Oscillators on Random Graphs

We describe a graph using an associated adjacency matrix $\mathbf{A}$ with elements A_{jk}. We assume that each of our graphs, which we assemble from random-graph models, are undirected, so their associated adjacency matrices are symmetric. We also assume that each graph has no self-edges (so $A_{jj} = 0$ for all j) and no multi-edges. Finally, we assume that our graphs are unweighted, so all entries of each matrix $\mathbf{A}$ are either 1 or 0.

To study dynamics on a graph, suppose that each node $j \in \{1, \ldots, N_s\}$ is associated with a Kuramoto oscillator [6]. This yields the following dynamical system:

$$\dot{\theta}_j = \omega_j + \frac{K}{N_s} \sum_{k=1}^{N_s} A_{jk} \sin(\theta_k - \theta_j)\,, \quad \omega_j \sim \frac{1}{\gamma} g\left(\frac{x}{\gamma}\right)\,, \tag{4}$$

where $\theta_j \in [0, 2\pi)$ is the phase of the jth oscillator, ω_j is the natural frequency of the jth oscillator, $K \geq 0$ controls the coupling strength between oscillators, and $g(y)$ is a mean probability distribution with mean 0 and width 1 (which constitutes a variance of 1, provided the variance of the distribution g is well-defined). Because of our rescaling, the parameter γ is the variance of the distribution; we obtain identical oscillators in the limit $\gamma \to 0^+$.

We are most interested in the extent to which the oscillators *lock*, which we characterize as

$$\lim_{t\to\infty} \theta_j(t) = \theta_p\,, \quad j \in \{1, \ldots, N_s\}\,, \tag{5}$$

in the strongest sense that we use in the present paper. The condition (5), in which θ_p is the common limiting phase of all oscillators, is called *phase locking*. One can

weaken the condition (5) and instead examine *frequency locking*, which entails that

$$\lim_{t\to\infty} \dot{\theta}_j(t) = \omega_f\,, \quad j \in \{1,\ldots,N_s\}\,.$$

In typical scenarios, phase locking implies frequency locking (although this need not be true in the presence of noise [29]), but the converse is not true in general.

To measure the extent that the oscillators lock, we calculate the order parameter

$$r_p(t)e^{i\psi_p(t)} = \frac{1}{N_s}\sum_{j=1}^{N_s} e^{i\theta_j(t)}\,,$$

and we note that $0 \le r_p(t) \le 1$. If the oscillators are equally spaced at time t, such that $\theta_j = \frac{2\pi(j-1)}{N_s}$, then

$$r_p(t)e^{i\psi_p(t)} = \frac{1}{N_s}\sum_{j=1}^{N_s}\left(e^{2\pi i/N_s}\right)^{(j-1)} = 0\,,$$

so $r_p(t) = 0$ indicates an absence of phase locking between the oscillators.

For frequency locking, it can be true that

$$\theta_j(t) \to \omega_f t + \theta_{j,s} \text{ as } t\to\infty\,,$$

where $\theta_{j,s}$ is a phase shift. In this case,

$$r_p(t)e^{i\psi_p(t)} \to e^{i\omega_f t}\frac{1}{N_s}\sum_{j=1}^{N_s} e^{i\theta_{j,s}}$$

as $t\to\infty$. It is then possible that $r_p(t)$ is small in magnitude because of the particular location of the phase shifts $\theta_{j,s}$. Nevertheless, there is much frequency locking among the oscillators.

If we meet the phase-locking criterion (5), then $r_p(t) \to 1$ and

$$r_p(t)e^{i\psi_p(t)} \to e^{i\theta_p} \text{ as } t\to\infty\,.$$

Therefore, $|r_p(t)|$ only provides unequivocal results for phase locking among the oscillators. As one may anticipate, and as we see in our numerical computations (see Section IV), it is rarely the case that calculating the order parameter $r_p(t)$ produces completely unambiguous results. Such insights have inspired previous efforts, such as the use of topological data analysis [30], to apply new data-analysis techniques to complement the investigation of order parameters in complex systems.

To help address this issue, we do perturbation theory to facilitate the interpretation of our later numerical results. We perturb with respect to the mean $\langle r_p\rangle$ of $r_p(t)$ over the time interval $[t_i, t_f]$. To compute this mean, we calculate

$$\langle r_p\rangle = \frac{1}{t_f - t_i}\int_{t_i}^{t_f} r_p(t)dt\,.$$

For frequency locking, a natural condition for our perturbations is to suppose as t becomes large that we can write each phase $\theta_j(t)$ in the form

$$\theta_j(t) = \omega_f t + \tilde{\theta}_j(\epsilon t)\,, \quad 0 < \epsilon \ll 1\,.$$

This framework allows slow modulations around the locking frequency, where the extent of the slowness is determined by the small positive parameter ϵ. We then see that

$$r_p(t) = \left|\frac{1}{N_s}\sum_{j=1}^{N_s} e^{i\theta_j(t)}\right| = \left|\frac{1}{N_s}\sum_{j=1}^{N_s} e^{i\tilde{\theta}_j(\epsilon t)}\right|\,,$$

which demonstrates that $r_p(t)$ varies slowly with respect to time. We then write the order parameter as $r_p(t) = \tilde{r}_p(\epsilon t)$, where

$$\tilde{r}_p(\epsilon t) = \left|\frac{1}{N_s}\sum_{j=1}^{N_s} e^{i\tilde{\theta}_j(\epsilon t)}\right|\,.$$

Making the reasonable assumption that $\tilde{r}_p(\epsilon t)$ has a well-defined derivative $\dot{\tilde{r}}_p(\epsilon t)$, we then compare $r_p(t)$ to the mean for $t \in [t_i, t_f]$ and write

$$\begin{aligned} r_p(t) - \langle r_p\rangle &= \frac{1}{t_f - t_i}\int_{t_i}^{t_f} \left(\tilde{r}_p(\epsilon t) - \tilde{r}_p(\epsilon s)\right) ds \\ &= \frac{1}{t_f - t_i}\int_{t_i}^{t_f} \left(\tilde{r}_p(\epsilon s + \epsilon(t-s)) - \tilde{r}_p(\epsilon s)\right) ds \\ &= \frac{\epsilon\dot{\tilde{r}}_p(\epsilon\xi)}{t_f - t_i}\int_{t_i}^{t_f}(t-s)ds\,, \quad \xi \in (t_i, t_f) \\ &= \dot{\tilde{r}}_p(\epsilon\xi)\left(\epsilon t - \epsilon\frac{(t_i + t_f)}{2}\right), \end{aligned} \tag{6}$$

where we used the mean-value theorem for the penultimate equality. This calculation shows that if oscillators vary slowly around a frequency-locked state, then the variation of the magnitude of the order parameter around the mean should (1) also be slow and (2) be bounded by the magnitude of the derivative multiplied by the difference between the time and the midpoint of the interval over which we average. As our numerical results demonstrate (see Section IV), frequency locking is more typical than phase locking for our networks of heterogeneous oscillators. Therefore, throughout the remainder of our paper, we make frequent recourse to the result in Eq. (6) of the above argument.

Similarly, we claim that a reasonable perturbation around a phase-locked state is

$$\theta_j(t) = \theta_p + \epsilon\tilde{\theta}_j(t)\,, \quad 0 < \epsilon \ll 1\,.$$

Using the Taylor-series expansion

$$e^{i\epsilon\tilde{\theta}_j} \approx 1 + i\epsilon\tilde{\theta}_j - \frac{\epsilon^2}{2}\tilde{\theta}_j^2$$

yields

$$r_p(t) \approx \left(1+\epsilon^2\left(\tilde{m}^2(t)-\frac{1}{N_s}\sum_{j=1}^{N_s}\tilde{\theta}_j^2(t)\right)\right)^{1/2}$$
$$\approx 1+\frac{\epsilon^2}{2}\left(\tilde{m}^2(t)-\frac{1}{N_s}\sum_{j=1}^{N_s}\tilde{\theta}_j^2(t)\right)$$
$$\approx 1-\frac{\epsilon^2}{2N_s}\sum_{j=1}^{N_s}\left(\tilde{\theta}_j(t)-\tilde{m}(t)\right)^2, \qquad (7)$$

where

$$\tilde{m}(t)=\frac{1}{N_s}\sum_{j=1}^{N_s}\tilde{\theta}_j(t)\,.$$

In the second line of (7), we used the Taylor-series approximation $\sqrt{1+x^2}\approx 1+x^2/2$. From Eq. (7), we can now clearly see how variances around the mean of the perturbations of the locked phase θ_p reduce the magnitude of the order parameter $r_p(t)$ below 1 and introduce temporal variations. We also anticipate that if we also allow the perturbations $\tilde{\theta}_j$ to vary slowly, then $r_p(t)$ should also vary slowly.

Finally, as was shown in [31], for Kuramoto oscillators on networks, there is necessarily some locking among some subset of the oscillators if

$$\gamma<\gamma_c\,,\quad \gamma_c=\frac{\pi N_s K g(0)\sigma^{\rm A}_{\rm max}}{2}\,,$$

where $\sigma^{\rm A}_{\rm max}$ is the largest eigenvalue of the adjacency matrix $\mathbf{A}$. However, the number of oscillators that lock (or the number of communities of oscillators that lock) is not clear from this single measurement. This is a difficult problem[6, 31], and these complexities have motivated much recent research on chimera states [32].

III. ESTIMATION OF LOCKING AND FUNCTIONAL-COMMUNITY DETECTION USING THE DYNAMIC-MODE DECOMPOSITION

To measure the amount of locking among the oscillators in the time interval $[t_i,t_f]$, we examine the collection $\{\xi_n\}_{n=1}^{N_r}$ of Koopman modes. We define the *overlap matrix* $\mathbf{C}^{\rm o}$ with elements

$$C^{\rm o}_{jl}=\left|\sum_{n=1}^{N_r}\hat{\xi}_{n,j}\hat{\xi}^*_{n,l}\right|\,,\quad \hat{\xi}_n=\frac{\xi_n}{\|\xi_n\|_2}\,.$$

Using the Cauchy–Schwarz inequality, we prove that

$$0\le C^{\rm o}_{jl}\le 1\,.$$

We also see that $\mathbf{C}^{\rm o}$ is symmetric. Using a threshold of $C_{\rm cr}\in(0,1)$, we construct graphs of the strongest interactions by generating an associated adjacency matrix $\mathbf{A}^{(\rm md)}(t_i,t_f)$ with elements

$$A^{(\rm md)}_{jl}(t_i,t_f)=\begin{cases}1\,, & C^{\rm o}_{jl}\ge C_{\rm cr}\\ 0\,, & C^{\rm o}_{jl}<C_{\rm cr}\,.\end{cases}\,.$$

The fact that $\mathbf{C}^{\rm o}$ is symmetric implies that $\mathbf{A}^{(\rm md)}(t_i,t_f)$ is symmetric and thus that its associated graph is undirected. In a given time interval, we define subsets of the oscillators to belong to a "community" if they are a part of the same connected component in this graph.

We expand on this notion of community to track the merging, separation, formation, and dissolution of communities over time. This adds then to a growing body of literature on detecting communities in time-varying networks; see, for example, [11, 33–35]. We separate a fixed time interval $[t_i,t_f]$ into n_w subintervals $\{I_j\}_{j=1}^{n_w}$ of equal length. We also generate n_w-1 equally spaced intervals $\left\{\tilde{I}_j\right\}_{j=1}^{n_w-1}$ that connect the midpoints of the I_j intervals. We order these intervals to give us a total of $2n_w-1$ intervals $\bar{I}_j$ such that

$$\bar{I}_j=\begin{cases}I_{(j+1)/2}\,, & 1\equiv j \bmod 2\\ \tilde{I}_{j/2}\,, & 0\equiv j \bmod 2\,.\end{cases}$$

With this construction, our collection of intervals overlaps in time. We generate a sequence of communities using the sequence

$$\left\{\mathbf{A}^{(\rm md)}(\bar{I}_j)\right\}_{j=1}^{2n_w-1}\,.$$

of adjacency matrices. We use overlapping time intervals to help ensure some continuity of the communities from one interval to the next. See [36] for further exploration of this issue.

To study how communities evolve over time, we define a time-dependent graph $\mathcal{G}_{t_i,t_f}$ that tracks community relationships across time. To generate this graph, for the first time interval $\bar{I}_1$, we use $\mathbf{A}^{(\rm md)}(\bar{I}_1)$ to obtain communities $\left\{C_k(\bar{I}_1)\right\}_{k=1}^{N_{c,1}}$ of oscillators in which each community corresponds to one connected component of the graph that is associated with $\mathbf{A}^{(\rm md)}(\bar{I}_1)$. Each of these communities corresponds to an individual node in $\mathcal{G}_{t_i,t_f}$. After initializing $\mathcal{G}_{t_i,t_f}$, we generate successive graphs in a sequence using the following recursive process. Assuming that we have constructed $\mathcal{G}_{t_i,t_f}$ up to the $j^{\rm th}$ time step, we place an edge between the $k^{\rm th}$ community $C_k(\bar{I}_j)$ from $\mathbf{A}^{(\rm md)}(\bar{I}_j)$ and the $l^{\rm th}$ community $C_l(\bar{I}_{j+1})$ from $\mathbf{A}^{(\rm md)}(\bar{I}_{j+1})$ if the nodes in $C_k(\bar{I}_j)$ are identical to or are a subset of those in $C_l(\bar{I}_{j+1})$. Otherwise, if the nodes in $C_k(\bar{I}_j)$ are not contained within a community or have fractured into smaller communities at the $(j+1)^{\rm th}$ time step, then $C_k(\bar{I}_j)$ terminates at the $j^{\rm th}$ time. This

process ensures that $\mathcal{G}_{t_i,t_f}$ is a forest that adaptively connects communities to each other across time based on the relative overlaps of Koopman modes. In our numerical computations (see Section IV), we observe coalescence of communities when there is phase locking or frequency locking.

In summary, our community-detection algorithm to generate $\mathcal{G}_{t_i,t_f}$ proceeds as follows:

Given a time series $\{\mathbf{y}_n\}_{n=1}^{N_s}$ in the time interval $[t_i, t_f]$

Require: Choose $C_{\rm cr}$ and n_w. Separate the interval $[t_i, t_f]$ into the overlapping subintervals $\left\{\bar{I}_j\right\}_{j=1}^{2n_w-1}$.

for $j \in \{1, \ldots, 2n_w - 1\}$ **do**

1. Compute the DMD of the part of the time series in the interval $\bar{I}_j$.
2. Compute the corresponding overlap matrix $\mathbf{C}^{\rm o}$ and its associated adjacency matrix $A^{(\rm md)}(\bar{I}_j)$ using the threshold $C_{\rm cr}$.
3. Compute the associated communities $\left\{C_k(\bar{I}_j)\right\}_{k=1}^{N_{c,j}}$. For each of the $N_{c,j}$ communities, add a node to $\mathcal{G}_{t_i,t_f}$.

if $j > 1$ **then**
for $k \in \{1, \ldots, N_{c,j}\}$ **do**
for $l \in \{1, \ldots, N_{c,j-1}\}$ **do**
if $C_k(\bar{I}_j) \subset C_l(\bar{I}_{j-1})$ **then**
Form an edge between the corresponding nodes in $\mathcal{G}_{t_i,t_f}$.
Break
end if
end for
end for
end if
end for

IV. NUMERICAL EXPERIMENTS

We now conduct a variety of numerical experiments to examine how well DMD does at detecting functional communities in networks of Kuramoto oscillators. Our networks have $N_s = 800$ oscillators, and the coupling parameter is $K = 10$. We draw the natural frequencies of the oscillators from a Gaussian distribution, so $\gamma_c = 4000\sqrt{\pi}\sigma^{\rm A}_{\rm max}$. Given this choice of distribution, we expect that at least subset of oscillators will always become at least nearly locked because $\sigma^{\rm A}_{\rm max} > 1$ in all of our experiments. We use a second-order Runge–Kutta solver with a step size of $\delta t = 0.05$ to integrate the Kuramoto model (4). We run all simulations up to $t_f = 800$. From $t = 760$ to $t_f = 800$, we perform DMD on the circle around which the oscillators move, so we use the coordinates $(\cos(\theta_j(t)), \sin(\theta_j(t)))$.

We set the DMD threshold in Eq. (3) to be $t_{\rm DMD} = -4$, the error threshold of the DMD modes to be $\epsilon_m = 10^{-1}$, and the reconstruction error to be $\epsilon_{\rm rc} = 10^{-1}$. As we described at the end of Section II A, these parameter choices reflect a balance that we obtain through trial and error. For our numerical experiments, we report results for heterogeneity parameters $\gamma = 0.1$, $\gamma = 1$, and $\gamma = 10$. Although smaller values of γ (indicating more homogeneous oscillators) allow greater viable ranges for these parameters, our choices represent values that hold up across the two decades of the range of values of γ that we examine.

In our simulations, we use two classical random-graph models (RGMs): the preferential-attachment (PA) model of Barabási–Albert (BA) [37] and the Watts–Strogatz (WS) small-world model [38]. After specifying the parameter values of an RGM, we generate a single graph from the model. When simulating the Kuramoto oscillators on either network, we initialize the dynamical system with N oscillators initially spaced uniformly around the circle. We now indicate the specific variants and parameter values that we present for these models. We also examined other parameter choices for these RGMs, and we obtain similar results.

For our BA network, we start with a seed network of $n = 10$ nodes with edges that we choose according to a $G(n, p)$ Erdős–Renyi (ER) model with an independent, uniform probability of $p = 0.75$ for placing an edge between nodes. At each time step, we add a new node to the network; this node has 4 edges that we connect uniformly at random (without replacement) to existing nodes. We grow our BA network until it consists of $N = 800$ nodes.

Our WS network also has $N = 800$ nodes. We start with a ring lattice in which each node is adjacent to $K_{\rm nn} = 20$ nearest neighbors. We then rewire the network as follows. Starting at the $j^{\rm th}$ node n_j, we consider half of its nearest-neighbor node n_l, where

$$l = \tilde{l} \bmod N\,, \quad j < \tilde{l} \leq j + \frac{K_{\rm nn}}{2}\,.$$

For each n_l, with probability β, we do the following.

1. We choose a node n_k uniformly at random from nodes that are not adjacent to n_j.
2. We remove the edge e_{jl} that connects n_j to n_l.
3. We add an undirected edge e_{jk} to connect n_j to n_k.

As we iterate through the nearest neighbors of n_j, we do not allow rewiring to any nodes that currently or formerly are nearest neighbors. However, such a nearest-neighbor connect can arise again when we rewire connections from other nodes after we have moved on from n_j. Therefore, it is possible for nearest-neighbor edges to be removed and added back again, although this is not a common event. In our simulations, we set the rewiring probability β to $\beta = 0.6$. As discussed in [1], the rewiring process drastically reduces the mean geodesic distance between nodes from that of the initial ring graph.

In our computations, we study the structure of the largest-connected component (LCC) in the adjacency

matrix $\mathbf{A}^{(\mathrm{md})}([760, 800])$. Our method of detecting functional communities always generates some output (regardless of whether it is interpretable), and it is instructive to examine the details of the predominant community that we obtain in the final examined time interval. We thereby improve our understanding of the meaning of the communities that we obtain using our approach. To help illustrate the structure of the LCC, we compare the local clustering coefficients of the LCC to those in the original RGM. For the j^{th} node of a network, we calculate the local clustering coefficient [1]

$$C_t(j) = \frac{\text{number of triangles through node } j}{\binom{d_j}{2}},$$

where d_j denotes the degree of node j. In Figure 1, we plot the local clustering coefficients of each node in networks that we construct using the BA and WS models. For most nodes, $C_t(j)$ is not particularly large for either RGM. Therefore, we do not expect to observe particularly modular structural communities in either RGM. In the WS model, the local clustering coefficients tend to be small because the rewiring probability is large.

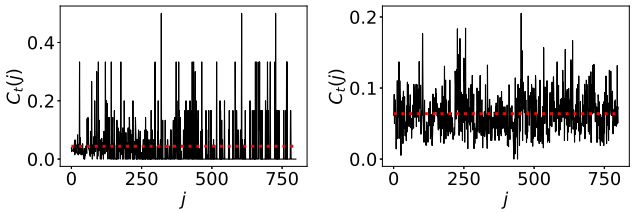

(a) (b)

FIG. 1. The local clustering coefficient $C_t(j)$ of each node j for (a) a Barabási–Albert (BA) network and (b) a Watts–Strogatz (WS) network. The horizontal line is the mean value of $C_t(j)$. Neither of these networks tends to have particularly large clustering coefficients, although the mean local clustering coefficient is larger in the WS network than in the BA network because of the nature of the associated RGMs.

To generate communities such as the LCC, we set the threshold of the correlation graph to be $C_{\mathrm{cr}} = 0.99$, except for the WS network with heterogeneity parameter $\gamma = 10$, where we use $C_{\mathrm{cr}} = 0.98$. We do this because the threshold $C_{\mathrm{cr}} = 0.99$ only yields one or two oscillators in the LCC, which makes it difficult to measure locking. Using a slightly smaller value of C_{cr} in this case ameliorates the issue and yields more intelligible results. Among the values of C_{cr} that we examined, our parameter choices typically produced the best community discrimination across the values of γ that we examined. Smaller values of C_{cr} generate fewer (and larger) communities; at large values of γ, this can allow too much heterogeneity within a community, and we then obtain little to no locking. For example, using $C_{\mathrm{cr}} = 0.95$ yields very similar results as $C_{\mathrm{cr}} = 0.99$ for $\gamma = 0.1$, but it yields communities with much less locking than for $C_{\mathrm{cr}} = 0.99$ when $\gamma = 1$ or $\gamma = 10$ in the BA model. Similar results hold for the WS model. Arguably, it may be desirable to allow the value of C_{cr} to change to adjust to the known heterogeneity (as quantified by γ) of the oscillators and produce communities with the most locking, but this increases the difficulty of comparing the functional communities that one obtains for different values of γ. Therefore, we use the value $C_{\mathrm{cr}} = 0.99$ for most of our case studies to facilitate exposition and consistency in reporting results.

As a final note about our parameter choices, we note that because we know about a key measurable aspect (which, in our case, is locking of the oscillators) of the underlying model, we are able to adjust our parameter choices to account for that phenomenon. Broadly, we expect our method to be useful for problems in which the dynamics include a similarly recognizable and quantifiable feature. There are a wide variety of ways in which one can define and identify these features in what one can term loosely as the task of "coherent-structure identification". See [39–41] for discussions of coherent structures in fluids and in other dynamical systems. However, without such features, our DMD approach is likely to produce arbitrary results that are difficult to analyze and verify, and we would not suggest using our method in such situations.

It is also worth considering other RGMs and multiple instances of an RGM for the same parameter values. We also did calculations with stochastic block models [1] and obtained results that are similar to those that we report in the paper. If one considers multiple instances of an RGM, one can then average over the $\mathbf{C}^{\mathrm{o}}$ matrices to obtain a consensus matrix and proceed to do community detection on the consensus matrix. This is an interesting question that is worth exploring in future work.

A. Weakly Heterogeneous Oscillators: $\gamma = 0.1$

We first consider oscillators that are only weakly heterogeneous by examining the case $\gamma = 0.1$. As one can see in Figures 2(a,b), in which we compare the distribution of oscillator frequencies $\dot{\theta}_j$ at $t = 0$ and $t = t_f = 800$, the mostly homogeneous natural frequencies of the oscillators lends itself to frequency locking. In these figures, we also observe differences that arise from the different network topologies of WS and BA networks. There is only a small amount of locking in the BA network, whereas the WS network is in an almost fully locked state. The similarity in the oscillators and relatively long simulation time in both networks generates a relatively modest number of DMD modes [see Figure 2(c,d)], with only about ten modes in each case.

Using $\mathbf{A}^{(\mathrm{md})}$, in Figure 3(a,b), we show the sizes of the communities that we generate with a given correlation-graph threshold. In both the BA and WS networks, the LCC is the largest community and almost all other oscillators belong to their own single-oscillator communities. As expected from the locking dynamics, the LCC is much

smaller in the BA network than in the WS network. In Figures 3(c,d), the mean local clustering coefficient in the BA network is smaller than that in the WS network. However, in both networks, the values of the local clustering coefficient are markedly larger in the LCC of $\mathbf{A}^{(\mathrm{md})}$ than in the original adjacency matrices of these networks. Compare Figures 3(c,d) to Figures 1(a,b).

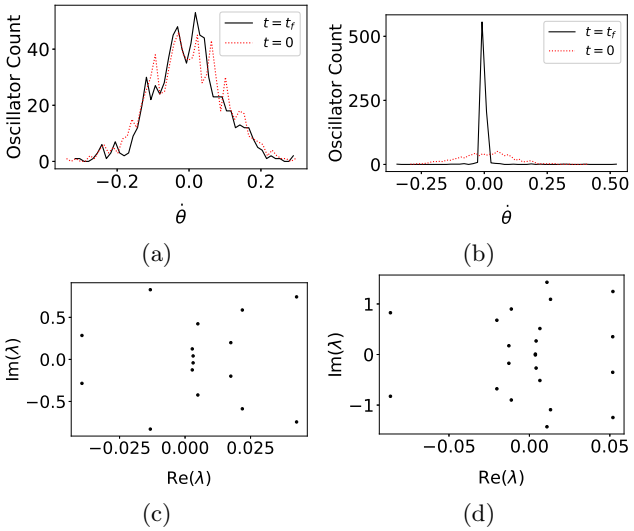

FIG. 2. (a,b) Frequency distributions and (c,d) DMD spectra for weakly heterogeneous Kuramoto oscillators (i.e., for $\gamma = 0.1$). We show our results for a BA network in the left column and for a WS network in the right column. In (a,b), we plot the distributions of $\dot{\theta}_j$ at $t = 0$ and $t = t_f$. Observe that the WS network clearly exhibits locking, whereas the BA network does not have a significant shift in the initial oscillator distribution. In (c,d), we show the associated DMD of these networks. The BA network has a smaller frequency range than in the WS network, as one can see in the values of Im(λ). Additionally, the larger range of Re(λ) values in the WS network than in the BA network indicate that the former experiences larger changes in amplitude.

In Figure 4, we plot the order parameters of the networks and LCCs of both the BA and WS networks. After applying our thresholding algorithm (see Algorithm 0), we see in Figures 4(e,f) that the order-parameter magnitude $r_p(t)$ oscillates less around the mean than in Figures 4(a,b). By comparing the real parts of the phases of the order parameter in Figures 4(c,g), we see that the LCC of the BA network has stronger frequency locking than the original network. By contrast, given that the original WS network is almost fully phase locked, its LCC only exhibits a little bit more phase locking [see Figures 4(d,h)].

B. Moderately Heterogeneous Oscillators: $\gamma = 1$

As we anticipate and confirm in our numerical computations, the small variance in the distribution of frequencies ω_j for $\gamma = 0.1$ case lends itself to the formation of locked states. The situation is starkly different when $\gamma = 1$ and the natural frequencies of the oscillators are much more heterogeneous. As we can see in Figures 5(a,b), there does not appear to a locked state on the same time scales as is the case for $\gamma = 0.1$. Additionally, the DMD spectra in Figures 5(c,d) now have about 50 modes, indicating a far greater complexity in the dynamics when $\gamma = 1$ than when $\gamma = 0.1$. This, in turn, results in much smaller functional communities [see Figures 6(a,b)]. Nevertheless, for both $\gamma = 0.1$ and $\gamma = 1$, the local clustering coefficients of the LCC of the $\mathbf{A}^{(\mathrm{md})}$ networks are much larger than those in the original networks.

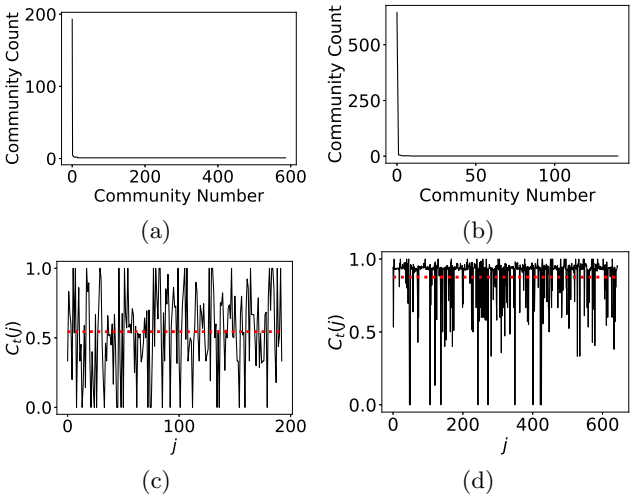

FIG. 3. (a,b) The numbers of nodes in each connected component of $\mathbf{A}^{(\mathrm{md})}$ and (c,d) the local clustering coefficients of the nodes in the LCC of $\mathbf{A}^{(\mathrm{md})}$ of the BA and WS networks for oscillators with $\gamma = 0.1$. We show our results for a BA network in the left column and for a WS network in the right column. In both the BA network and the WS network, the LCC is the largest community by far. Additionally, in both networks, the local clustering coefficients of the nodes in the LCC of $\mathbf{A}^{(\mathrm{md})}$ are markedly larger than the baseline values in the original networks in Figure 1.

This clear absence of locking is echoed in Figures 7(a,b), which reveal that the order-parameter magnitudes $r_p(t)$ are markedly more oscillatory when $\gamma = 1$ than they are for $\gamma = 0.1$. Additionally, we do not observe steady oscillations in $\cos(\psi_p(t))$ [see Figures 7(c,d)]. However, in the LCC of $\mathbf{A}^{(\mathrm{md})}$, the oscillations of $r_p(t)$ around the mean are markedly smaller for $\gamma = 1$ [see Figures 7(e,f)] than for $\gamma = 0.1$, which [by using Eq. (6)] we can attribute to the much stronger frequency locking when $\gamma = 1$. The far steadier and uniformly oscillating phase in Figures 7(g,h) than we observed for $\gamma = 0.1$ corroborates this result, although the BA network does exhibit some fast phase dynamics towards the end of our simulation. This may suggest that the frequency locking is not entirely stable. Such dynamics merit further exploration in future efforts to gain a thorough understanding of why they occur.

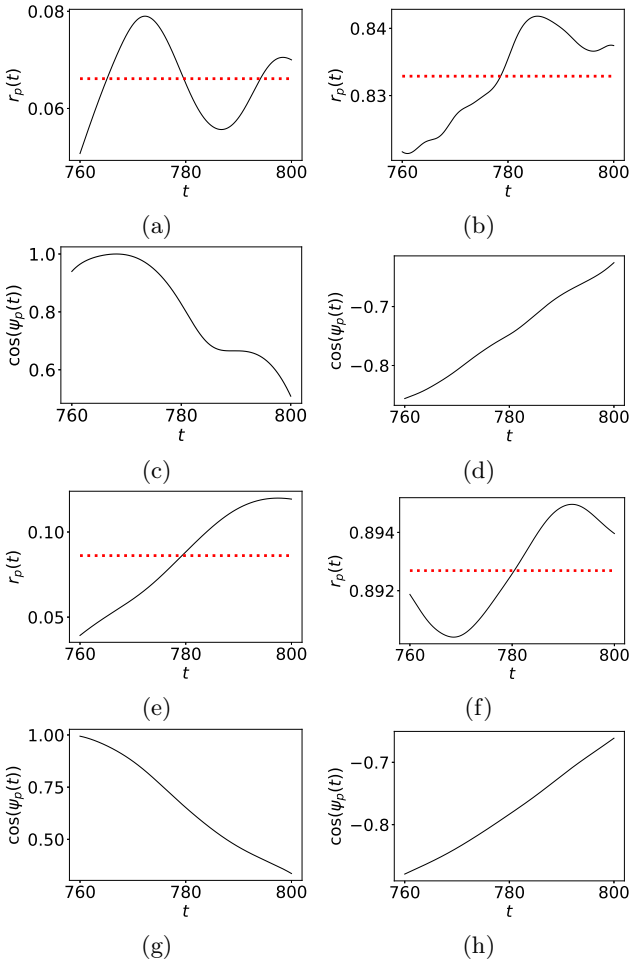

FIG. 4. The (a,b,e,f) order-parameter magnitude $r_p(t)$ and (c,d,g,h) real part $\cos(\psi_p(t))$ of the order-parameter phase for the BA and WS networks with weakly heterogeneous oscillators (i.e., for $\gamma = 0.1$). We show our results for a BA network in the left column and for a WS network in the right column. Our results for the original two networks are in panels (a)–(d), and our results for the LCCs of $\mathbf{A}^{(\mathrm{md})}$ of these networks are in (e)–(h). The horizontal line in (a,b,e,f) indicates the mean $\langle r_p(\cdot)\rangle$ of the order-parameter magnitude. For the BA model, we observe stronger frequency locking in the LCC of $\mathbf{A}^{(\mathrm{md})}$ than in the original network because the former has slower variations in $r_p(t)$ around the mean and more regular behavior of the phase. In the WS model, we see evidence that the LCC of $\mathbf{A}^{(\mathrm{md})}$ has more phase locking than the original network.

C. Strongly Heterogeneous Oscillators: $\gamma = 10$

Finally, we examine strongly heterogeneous oscillators by setting $\gamma = 10$. Recall that we use a threshold of $C_{\mathrm{cr}} = 0.99$ for the BA model and a threshold of $C_{\mathrm{cr}} = 0.98$ for the WS model. We use a smaller threshold for the WS model to ensure that there are enough oscillators in the LCC to obtain meaningful measurements. Based on our previous results, we anticipate that we are unlikely to observe locking among any significant frac-

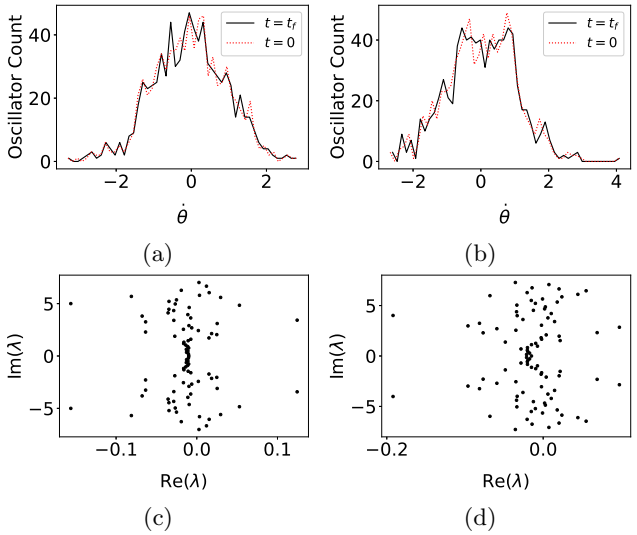

FIG. 5. (a,b) Frequency distributions and (c,d) DMD spectra for moderately heterogeneous Kuramoto oscillators (i.e., for $\gamma = 1$). We show our results for a BA network in the left column and for a WS network in the right column. In (a,b), we plot the distributions of $\dot{\theta}_j$ at $t = 0$ and $t = t_f$ for (a) a BA network and (b) a WS network. For $\gamma = 1$, the characteristics of the networks from the two RGMs are much less distinguishable than is the case for $\gamma = 0.1$. However, the DMD spectra still have some differences, such as how eigenvalues cluster on the imaginary axis.

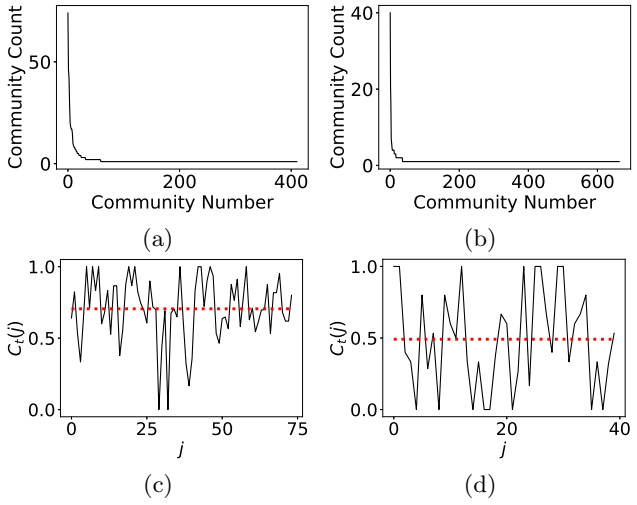

FIG. 6. (a,b) The numbers of nodes in each connected component of $\mathbf{A}^{(\mathrm{md})}$ and (c,d) the local clustering coefficients of the nodes in the LCC of $\mathbf{A}^{(\mathrm{md})}$ of the BA and WS networks for oscillators with $\gamma = 1$. We show our results for a BA network in the left column and for a WS network in the right column. The LCCs are still markedly larger than any other community, but they are much smaller than they are for $\gamma = 0.1$. In both networks, the local clustering coefficients of the nodes in the LCC of $\mathbf{A}^{(\mathrm{md})}$ are again markedly larger than the baseline values in the original networks in Figure 1, although this is now less extreme than is the case for $\gamma = 0.1$.

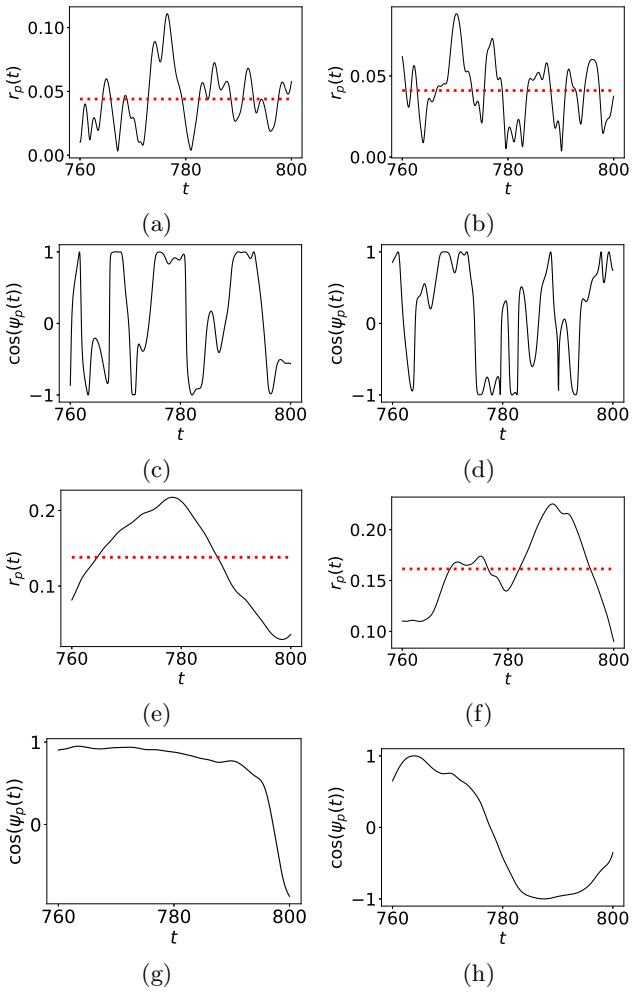

FIG. 7. The (a,b,e,f) order-parameter magnitude $r_p(t)$ and (c,d,g,h) real part $\cos(\psi_p(t))$ of the order-parameter phase for the BA and WS networks for $\gamma = 1$. Our results for the original two networks are in panels (a)–(d), and our results for the LCCs of $\mathbf{A}^{(\mathrm{md})}$ of these networks are in panels (e)–(h). We show our results for a BA network in the left column and for a WS network in the right column. The horizontal line in (a,b,e,f) indicates the mean $\langle r_p(\cdot)\rangle$ of the order-parameter magnitude. For both the BA network and the WS network, the LCC of $\mathbf{A}^{(\mathrm{md})}$ has much stronger frequency locking [as one can see by the slow variation in both $r_p(t)$ and $\cos(\psi_p(t))$] than in the original networks, although the BA network appears to exhibit somewhat different dynamics towards the end of the simulation.

tion of the oscillators on the time scales that we examine. Our computations in Figure 8 confirm this expectation. From the distributions of the frequencies in Figures 8(a,b), we see that there is almost no change in the distributions during our simulations. This yields the complicated DMD spectra, with approximately 340 eigenvalues for each network, in Figures 8(c,d). The community counts in Figures 9(a,b) reveal that even the LCCs of $\mathbf{A}^{(\mathrm{md})}$ only have 7 oscillators for each network. However, as one can see in Figures 9(c,d), these LCCs still have larger values of $C_t(j)$ than the original networks.

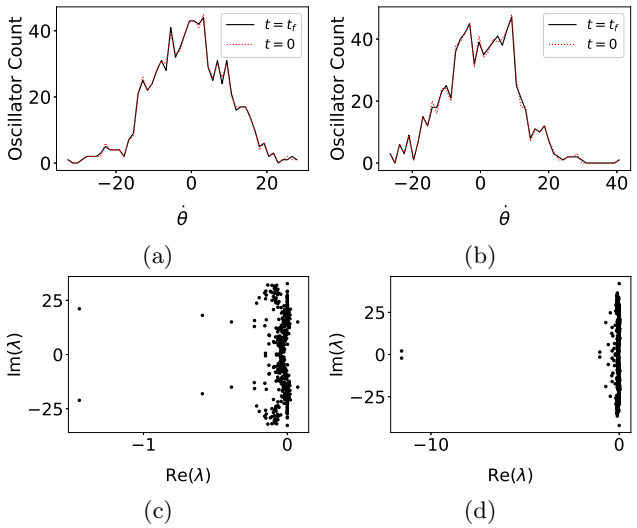

FIG. 8. (a,b) Frequency distributions and (c,d) DMD spectra for strongly heterogeneous Kuramoto oscillators (i.e., for $\gamma = 10$). We show our results for a BA network in the left column and for a WS network in the right column. In (a,b), we plot the distributions of $\dot{\theta}_j$ at $t = 0$ and $t = t_f$ for (a) a BA network and (b) a WS network. It is now difficult to distinguish between the networks from the two models, although we still observe slight differences in the DMD spectra.

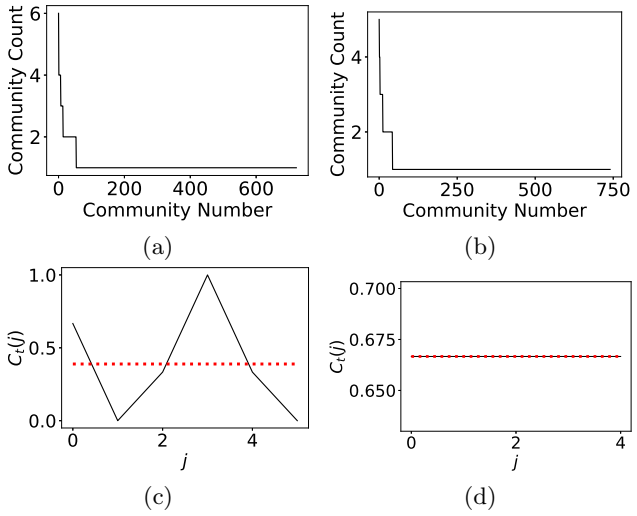

FIG. 9. (a,b) The numbers of nodes in each connected component of $\mathbf{A}^{(\mathrm{md})}$ and (c,d) the local clustering coefficients of the nodes in the LCC of $\mathbf{A}^{(\mathrm{md})}$ of the BA and WS networks for oscillators with $\gamma = 10$. We show our results for a BA network in the left column and for a WS network in the right column. The large spread in oscillator frequencies for these strongly heterogeneous oscillators prevents the formation of large LCCs, and no community has more than a few oscillators in it. Nevertheless, the local clustering coefficients of the nodes in the LCC of $\mathbf{A}^{(\mathrm{md})}$ are still larger than the baseline values in the original networks in Figure 1.

In Figure 10, we see that the functional community of oscillators that consists of the LCC of $\mathbf{A}^{(\mathrm{md})}$ is markedly closer to being frequency locked than those oscillators are in the original network. This arises from the larger, less oscillatory values of r_p and less erratic dynamics of $\cos(\psi_p(t))$ in Figures 10(e)–(h) than in Figures 10(a)–(d). Therefore, although few oscillators are in these communities for $\gamma = 10$ (with the vast majority of oscillators wandering incoherently), these lucky few oscillators are very close to being locked together.

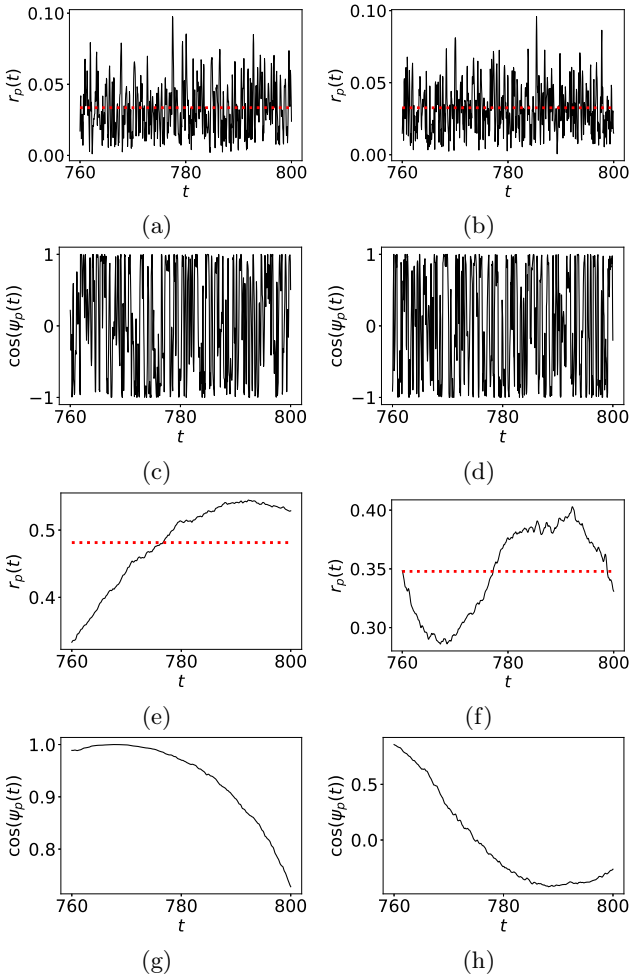

FIG. 10. The (a,b,e,f) order-parameter magnitude $r_p(t)$ and (c,d,g,h) real part $\cos(\psi_p(t))$ of the order-parameter phase for the BA and WS networks for $\gamma = 10$. Our results for the original two networks are in panels (a)–(d), and our results for the LCCs of $\mathbf{A}^{(\mathrm{md})}$ of these networks are in panels (e)–(h). We show our results for a BA network in the left column and for a WS network in the right column. The horizontal line in (a,b,e,f) indicates the mean $\langle r_p(\cdot)\rangle$ of the order-parameter magnitude. The networks from both models exhibit more frequency locking in the LCC of $\mathbf{A}^{(\mathrm{md})}$ than in the original networks.

D. Community Dynamics

Now that we have established that our method of generating functional communities of oscillators in a manner that is consistent with their dynamics, we compare how communities form for $\gamma = 0.1$ (i.e., the case of weakly heterogeneous oscillators) in the two RGMs. In Figure 11, we see that community formation occurs in starkly different ways in the two models, as the BA network has a far weaker tendency towards community coalescence than the WS network. We also see in the BA network that communities can cease to propagate in time, as there is often a sequence of coalescing communities that then stop propagating further. Therefore, we see that our notion of functional communities allows us to examine their temporal evolution and to thereby capture some details of the dynamics of the coupled oscillators.

V. CONCLUSIONS AND DISCUSSION

Using DMD, we developed a versatile approach for identifying functional communities of heterogeneous coupled oscillators on networks. Specifically, we examined coupled Kuramoto oscillators on networks that we constructed from random-graph models, and we found functional communities of oscillators based on how much they exhibit phase locking and frequency locking. These functional communities arise through clustering in graphs of community relationships, and the clustering coefficients in these graphs are larger than the clustering coefficients in the original networks. Unsurprisingly, in concert with associated synchronization properties, these functional communities are stronger for networks of weakly heterogeneous oscillators than they are for networks of strongly coupled oscillators. The community-relationship graphs, which take the form of forests, encode the interactions between the oscillators and provide a way to visualize their complicated dynamics over time. We observed coalescence of communities when oscillators exhibit phase locking or frequency locking. Additionally, from our community-relationship graphs, we observed that BA networks and WS networks yield functional communities with different community-coalescence properties.

Our results seem are promising, and it is important to test them in increasingly challenging scenarios. The dynamical-systems community loves the Kuramoto model (and we specifically are certainly fond of it), and the fact that it is so well-studied [6] makes it a very helpful starting point for developing approaches like ours. However, it is desirable to challenge our approach with other models of coupled oscillators, other dynamical systems, and time-series output of natural observations and laboratory experiments.

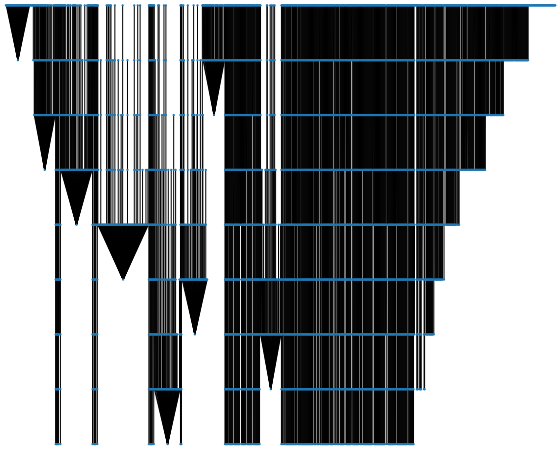

(a) BA model

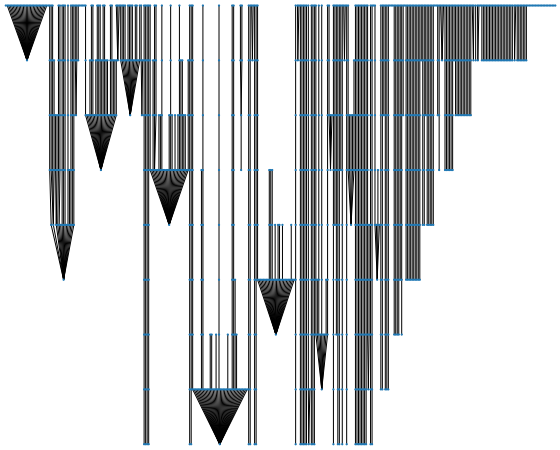

(b) WS model

FIG. 11. The community-relationship graphs $\mathcal{G}_{t_i,t_f}$ for weakly heterogeneous oscillators (i.e., $\gamma = 0.1$) for (a) a BA network and (b) a WS network for the time interval $t_i = 600 \leq t \leq t_f = 800$ across overlapping intervals of 40 time units (i.e., with $n_w = 5$). Time runs from top to bottom. This plot illustrates how functional communities, which consist of oscillators with similar dynamics, evolve over time.

ACKNOWLEDGEMENTS

We thank Arkady Pikovsky for helpful comments.

[1] M. E. J. Newman. *Networks*. Oxford University Press, Oxford, UK, 2nd edition, 2018.

[2] M. A. Porter and J. P. Gleeson. *Dynamical Systems on Networks: A Tutorial*. Frontiers in Applied Dynamical Systems: Reviews and Tutorials. Springer International Publishing, 2016.

[3] I. Z. Kiss, J. C. Miller, and P. L. Simon. *Mathematics of Epidemics on Networks: From Exact to Approximate Models*. Springer International Publishing, Cham, Switzerland, 2017.

[4] S. Lehmann and Y.-Y. Ahn. *Complex Spreading Phenomena in Social Systems: Influence and Contagion in Real-World Social Networks*. Springer International Publishing, Cham, Switzerland, 2018.

[5] A. Arenas, A. Díaz-Guilera, J. Kurths, Y. Moreno, and C. Zhou. Synchronization in complex networks. *Physics Reports*, 469:93–153, 2008.

[6] F. A. Rodgrigues, T. K. DM. Peron, P. Ji, and J. Kurths. The Kuramoto model in complex networks. *Physics Reports*, 610:1–98, 2016.

[7] M. A. Porter. Nonlinearity + Networks: A 2020 vision. In P. G. Kevrekidis, J. Cuevas-Maraver, and A. Saxena, editors, *Emerging Frontiers in Nonlinear Science*, pages 131–159. Springer International Publishing, Cham, Switzerland, 2020.

[8] M. A. Porter, J.-P. Onnela, and P. J. Mucha. Communities in networks. *Notices of the American Mathematical Society*, 56:1082–1097, 1164–1166, 2009.

[9] S. Fortunato and D. Hric. Community detection in networks: A user guide. *Physics Reports*, 659:1–44, 2016.

[10] A. Arenas, A. Díaz-Guilera, and C. J. Pérez-Vicente. Synchronization reveals topological scales in complex networks. *Physical Review Letters*, 96:114102, 2006.

[11] D. S. Bassett, M. A. Porter, N. F. Wymbs, S. T. Grafton, J. M. Carlson, and P. J. Mucha. Robust detection of dynamic community structure in networks. *Chaos*, 23:013142, 2013.

[12] S. Chauhan, M. Girvan, and E. Ott. A network function-based definition of communities in complex networks. *Chaos*, 22(3):033129, 2012.

[13] S. Boccaletti, M. Ivanchenko, V. Latora, A. Pluchino, and A. Rapisarda. Detecting complex network modularity by dynamical clustering. *Physical Review E*, 75:045102, 2007.

[14] J. Wu and Y. Jiao. Clustering dynamics of complex discrete-time networks and its application in community detection. *Chaos*, 24:033104, 2014.

[15] C. R. Shalizi, M. F. Camperi, and K. L. Klinkner. Discovering functional communities in dynamical networks. In E. Airoldi, D. M. Blei, S. E. Fienberg, A. Goldenberg, E. P. Xing, and A. X. Zheng, editors, *Statistical Network Analysis: Models, Issues, and New Directions*, pages 140–157, Heidelberg, Germany, 2007. Springer-Verlag.

[16] P. Schmid. Dynamic mode decomposition of numerical and experimental data. *Journal of Fluid Mechanics*, 656:5–28, 2010.

[17] I. Mezić. Spectral properties of dynamical systems, model reduction, and decompositions. *Nonlinear Dynics*, 41:309–325, 2005.

[18] J. N. Kutz, S. L. Brunton, B. W. Brunton, and J. L. Proctor. *Dynamic Mode Decomposition: Data-Driven Modeling of Complex Systems*. SIAM, Philadelphia, PA, USA, 2016.

[19] K. Taira, S. L. Brunton, S. T. M. Dawson, C. W. Rowley, T. Colonius, B. J. McKeon, O. T. Schmidt, S. Gordeyev, V. Theofilis, and L.S. Ukeiley. Modal analysis of fluid flows: An overview. *AIAA Journal*, 55:4013–4041, 2017.

[20] S. Le Clainche and J. M. Vega. Analyzing nonlinear dynamics via data-driven dynamic mode decomposition-like methods. *Complexity*, 2018:6920783, 2018.

[21] S. L. Brunton, M. Budišić, E. Kaiser, and J. N. Kutz. Modern Koopman theory for dynamical systems. *arXiv:2102.12086*, 2021.

[22] B. O. Koopman. Hamiltonian systems and transformation in Hilbert space. *Proceedings of the National Academy of Sciences f the United States of America*, 17:315–318, 1931.

[23] J. M. Kunert-Graf, K. M. Eschenburg, D. J. Galas, J. N. Kutz, S. D. Rane, and B. W. Brunton. Extracting reproducible time-resolved resting state networks. *Frontiers in Computational Neuroscience*, 13:75, 2019.

[24] M. O. Williams, I. G. Kevrekidis, and C. W. Rowley. A data-driven approximation of the Koopman operator: Extending dynamic mode decomposition. *Journal of Nonlinear Science*, 25:1307–1346, 2015.

[25] M. O. Williams, C. W. Rowley, and I. G. Kevrekidis. A kernel-based method for data driven Koopman spectral analysis. *Journal of Computational Dynamics*, 2:247–265, 2015.

[26] C. D. Martin and M. A. Porter. The extraordinary SVD. *American Mathematical Monthly*, 119:838–851, 2012.

[27] M.S. Hemati, C. W. Rowley, E. A. Deem, and L. N. Cattafesta. De-biasing the dynamic mode decomposition for applied Koopman spectral analysis of noisy data. *Theor. Comput. Fluid Dyn.*, 31:349–368, 2017.

[28] H. Zhang, S. T. M. Dawson, C. W. Rowley, E. A. Deem, and L. N. Cattafesta. Evaluating the accuracy of the dynamic mode decomposition. *Journal of Computational Dynamics*, 7:35–56, 2020.

[29] A. V. Pimenova, D. S. Goldobin, M. Rosenblum, and A. Pikovsky. Interplay of coupling and common noise at the transition to synchrony in oscillator populations. *Scientific Reports*, 6:38518, 2016.

[30] C. M. Topaz, L. Ziegelmeier, and T. Halverson. Topological data analysis of biological aggregation models. *PLOS ONE*, 10(5):e0126383, 05 2015.

[31] J. G. Restrepo, E. Ott, and B. R. Hunt. Onset of synchronization in large networks of coupled oscillators. *Physical Review E*, 71:036151, 2005.

[32] M. J. Panaggio and D. M. Abrams. Chimera states: Coexistence of coherence and incoherence in networks of coupled oscillators. *Nonlinearity*, 28(3):R67–R87, 2015.

[33] G. Palla, A.-L. Barabási, and T. Vicsek. Quantifying social group evolution. *Nature*, 446:664–667, 2007.

[34] P. J. Mucha, T. Richardson, K. Macon, M. A. Porter, and J.-P. Onnela. Community structure in time-dependent, multiscale, and multiplex networks. *Science*, 328(5980):876–878, 2010.

[35] P. Holme. Modern temporal network theory: A colloquium. *European Physical Journal B*, 8:234, 2015.

[36] D. J. Fenn, M. A. Porter, P. J. Mucha, M. McDonald, S. Williams, N.F. Johnson, and N. S. Jones. Dynamical clustering of exchange rates. *Quantitative Finance*, 12:1493–1520, 2012.

[37] A.-L. Barabási and R. Albert. Emergence of scaling in random networks. *Science*, 286(5439):509–512, 1999.

[38] D. J. Watts and S. H. Strogatz. Collective dynamics of 'small-world' networks. *Nature*, 393:440–442, 1998.

[39] G. Haller. Lagrangian coherent structures. *Annual Review of Fluid Mechanics*, 47(1):137–162, 2015.

[40] M. R. Allshouse and T. Peacock. Lagrangian based methods for coherent structure detection. *Chaos*, 25(9):097617, 2015.

[41] P. Holmes, J.L. Lumley, G. Berkooz, and C.W. Rowley. *Turbulence, Coherent Structures, Dynamical Systems and Symmetry*. Cambridge University Press, Cambridge, UK, 2nd edition, 2012.